



## NRC Publications Archive Archives des publications du CNRC

### **Energy level alignment at hybridized organic–metal interfaces: the role of many-electron effects**

Chen, Yifeng; Tamblyn, Isaac; Quek, Su Ying

This publication could be one of several versions: author's original, accepted manuscript or the publisher's version. / La version de cette publication peut être l'une des suivantes : la version prépublication de l'auteur, la version acceptée du manuscrit ou la version de l'éditeur.

For the publisher's version, please access the DOI link below. / Pour consulter la version de l'éditeur, utilisez le lien DOI ci-dessous.

#### **Publisher's version / Version de l'éditeur:**

<https://doi.org/10.1021/acs.jpcc.7b00715>

*The Journal of Physical Chemistry C*, 121, 24, pp. 13125-13134, 2017-05-19

#### **NRC Publications Record / Notice d'Archives des publications de CNRC:**

<https://nrc-publications.canada.ca/eng/view/object/?id=f4633608-47d7-429b-aacb-5ae334d279a7>

<https://publications-cnrc.canada.ca/fra/voir/objet/?id=f4633608-47d7-429b-aacb-5ae334d279a7>

Access and use of this website and the material on it are subject to the Terms and Conditions set forth at

<https://nrc-publications.canada.ca/eng/copyright>

READ THESE TERMS AND CONDITIONS CAREFULLY BEFORE USING THIS WEBSITE.

L'accès à ce site Web et l'utilisation de son contenu sont assujettis aux conditions présentées dans le site

<https://publications-cnrc.canada.ca/fra/droits>

LISEZ CES CONDITIONS ATTENTIVEMENT AVANT D'UTILISER CE SITE WEB.

**Questions?** Contact the NRC Publications Archive team at

PublicationsArchive-ArchivesPublications@nrc-cnrc.gc.ca. If you wish to email the authors directly, please see the first page of the publication for their contact information.

**Vous avez des questions?** Nous pouvons vous aider. Pour communiquer directement avec un auteur, consultez la première page de la revue dans laquelle son article a été publié afin de trouver ses coordonnées. Si vous n'arrivez pas à les repérer, communiquez avec nous à PublicationsArchive-ArchivesPublications@nrc-cnrc.gc.ca.

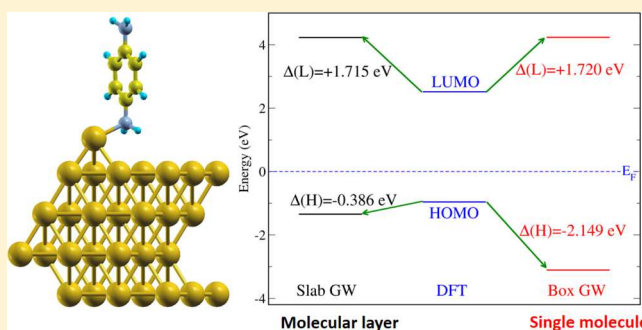


# Energy Level Alignment at Hybridized Organic–Metal Interfaces: The Role of Many-Electron Effects

Yifeng Chen,<sup>†</sup> Isaac Tamblyn,<sup>‡,§</sup> and Su Ying Quek<sup>\*,†,||</sup><sup>†</sup>Centre for Advanced 2D Materials and Graphene Research Centre, National University of Singapore, 6 Science Drive 2, Singapore 117542<sup>‡</sup>National Research Council of Canada, 100 Sussex Drive, Ottawa, Ontario K1A 0R6, Canada<sup>§</sup>Department of Physics, University of Ontario Institute of Technology, Oshawa, Ontario L1H 7K4, Canada<sup>||</sup>Department of Physics, National University of Singapore, 2 Science Drive 3, Singapore 117551

## Supporting Information

**ABSTRACT:** Hybridized molecule/metal interfaces are ubiquitous in molecular and organic devices. The energy level alignment (ELA) of frontier molecular levels relative to the metal Fermi level ( $E_F$ ) is critical to the conductance and functionality of these devices. However, a clear understanding of the ELA that includes many-electron self-energy effects is lacking. Here, we investigate the many-electron effects on the ELA using state-of-the-art, benchmark GW calculations on prototypical chemisorbed molecules on Au(111), in eleven different geometries. The GW ELA is in good agreement with photoemission for monolayers of benzene diamine on Au(111). We find that in addition to static image charge screening, the frontier levels in most of these geometries are renormalized by additional screening from substrate-mediated intermolecular Coulomb interactions. For weakly chemisorbed systems, such as amines and pyridines on Au, this additional level renormalization ( $\sim 1.5$  eV) comes solely from static screened exchange energy, allowing us to suggest computationally more tractable schemes to predict the ELA at such interfaces. However, for more strongly chemisorbed thiolate layers, dynamical effects are present. Our ab initio results constitute an important step toward the understanding and manipulation of functional molecular/organic systems for both fundamental studies and applications.



## 1. INTRODUCTION

Molecules in both monolayer and single-molecule forms constitute basic building blocks for molecular and organic electronics.<sup>1–4</sup> The energy level alignment (ELA) between the metal electrode Fermi level ( $E_F$ ) and frontier molecular orbital (MO) levels determines the energy barrier faced by electrons tunneling across the interface, thus having a critical impact on electronic and charge transport properties.<sup>5,6</sup> For example, a change in the ELA of  $\sim 1$  eV can change the conductance in single-molecule junctions by an order of magnitude.<sup>7,8</sup> Experimentally, the ELA at molecule/metal interfaces can be determined by photoemission experiments, but correlating the ELA with atomistic-scale knowledge of the interface geometry can be challenging. To directly relate atomic geometries with ELA is highly desirable, underscoring the need to develop accurate theoretical methods to predict the ELA at such interfaces, as well as to develop a basic understanding of the essential physics governing the ELA. However, quantitative prediction of the ELA is nontrivial for hybridized molecule/metal interfaces where wave functions are spatially distributed across the interface. Molecules and metals have very different electronic structures, and it is difficult to treat both on the same

footing while retaining their respective accuracy. Density functional theory (DFT) methods are routinely unable to predict the correct ELA and also give incorrect wave functions due to inaccurate mixing of the molecule and metal states. Local and semilocal approximations to the exchange–correlation functional typically underestimate molecular highest occupied molecular orbital (HOMO)–lowest unoccupied molecular orbital (LUMO) gaps by several eVs. Hybrid functional calculations reduce this error, but the optimal percentage of exact exchange in the functional for molecules is different from that for metals. Many-electron GW calculations can correct the band gap problem in DFT, predicting quantitatively accurate band gaps for semiconductors<sup>9,10</sup> and HOMO–LUMO gaps for molecules.<sup>11</sup> Unlike many hybrid functionals, the GW calculations do not rely on empirical fits and also include the self-energy effects due to screening from the environment.<sup>12–14</sup> In contrast to DFT (a mean-field approach), many-electron GW calculations also provide ab initio insights into the electron

Received: January 23, 2017

Revised: May 19, 2017

Published: May 19, 2017

self-energy effects at the interface. However, GW calculations are computationally prohibitive for large systems. As a result, very little has been done to understand from first-principles the many-electron self-energy effects governing the ELA at hybridized molecule/metal interfaces.

Electron transport in molecule/metal interface systems has been intensively investigated experimentally, for both molecular self-assembled monolayers (SAMs) and single-molecular systems. These studies are performed in the context of SAM junctions, realized by contacting the monolayer with a top electrode,<sup>15,16</sup> and single-molecule junctions in scanning tunneling microscopy based experiments or mechanically controlled break junction experiments,<sup>7,8,17–20</sup> all of which involve hybridized molecule/metal interfaces, where the MOs of interest overlap with metal states. DFT calculations at the level of semilocal exchange-correlation functionals have provided much insight into these systems, showing the ELA to be affected by a complex interplay between charge transfer, local charge rearrangements, bond dipoles, depolarization fields, and Pauli pushback effects.<sup>21–26</sup> On the other hand, it has been shown that DFT with standard exchange-correlation functionals cannot account for all the physics at molecule/metal interfaces. Specifically, for physisorbed molecule/metal interfaces (which do not have hybridization effects), many-electron GW calculations have identified a large substrate-induced renormalization of the MO levels, which has been attributed to nonlocal static image charge screening from the substrate.<sup>13,14,27</sup> This information has enabled the prediction of ELA at physisorbed molecule/metal interfaces using a simple two-step DFT+ $\Sigma$  approach, which combines gas-phase self-energies with substrate-induced image charge energies.<sup>13,14,27,28</sup>

Despite the success of the simple picture of image charge screening known for physisorbed systems, hybridization can potentially change the many-electron screening effects significantly. At hybridized molecule/metal interfaces, molecules form chemical bonds with the metal substrates, with the possibility of charge rearrangements. The wave functions of the combined system become a superposition of molecular orbitals and metal states. If bonds in the molecule are broken upon chemisorption, this stronger hybridization complicates the picture further. What are the many-electron screening effects at hybridized molecule/metal interfaces? How does hybridization change the picture of static image charge screening? Is it possible to predict the ELA at hybridized molecule/metal interfaces without computationally expensive GW calculations?

Here, we shed light on the many-electron exchange and correlation effects (i.e., electronic self-energy effects) on the ELA at hybridized molecule/metal interfaces by performing state-of-the-art GW calculations for prototypical small  $\pi$ -conjugated molecules on Au(111) with common anchoring groups (amine, pyridine, and thiol), in eleven different geometries. Comparison is made with the DFT+ $\Sigma$  (image charge screening) approach to facilitate our analysis of the many-electron screening effects at these interfaces. In particular, as a measure of the self-energy effects that go beyond gas-phase exchange/correlation and simple image charge screening, we define  $\Lambda$  as the difference between the ELAs obtained with GW and DFT+ $\Sigma$  (magnitude of GW level minus DFT+ $\Sigma$  level). Interestingly, we find that  $\Lambda$  is very large (close to 1.5 eV) for molecular layers, but  $\Lambda$  is close to zero when intermolecular Coulomb interactions are removed in the evaluation of the self-energy (“single-molecule limit”). The large  $\Lambda$  for molecular layers brings the frontier levels much closer to  $E_F$ , and the

resulting net GW self-energy correction for hybridized molecular layers on Au is relatively small (<0.5 eV) compared to that in physisorbed molecule/metal layers.<sup>13,14,27</sup> However, this  $\sim 0.5$  eV correction can still result in a significant change in the frontier MO level relative to  $E_F$ , as it can remove apparent Fermi level pinning observed at the DFT level for thiolates on Au. We note that the large  $\Lambda$  also results in a smaller HOMO–LUMO gap for the molecular layers, compared to that predicted from image charge screening. On the other hand, the close-to-zero  $\Lambda$  for the single-molecule limit is consistent with the success of the DFT+ $\Sigma$  approach in predicting the conductance of single-molecule junctions.<sup>7,8,29–31</sup> This shows that static image charge effects can account for most of the substrate-induced self-energy effects in single-molecule junctions, even in the presence of hybridization. The additional level renormalization (beyond static image charge screening) for molecular layers is thus related to intermolecular Coulomb interactions in the evaluation of the self-energy of the hybridized system. The physical origin of this additional renormalization can be traced to static screened exchange for amines and pyridines on Au. This result suggests a way to predict the ELA at such interfaces without GW calculations. However, the self-energy effects are more complicated for the more strongly bound thiolate/Au interfaces, where bonds in the molecule are broken upon adsorption.

## 2. METHODS

**2.1. Density Functional Theory Calculations.** To relax our hybridized molecule–metal slab geometries, we have used both PBE-D2<sup>32</sup> and vdW-DF2<sup>33,34</sup> exchange-correlation functionals, to take into account van der Waals interactions. We have used both functionals to relax geometry **1** and note that the GW ELA is not sensitive to the choice of PBE-D2 versus vdW-DF2 for geometry optimization. Geometry **3** and systems with thiols are relaxed fully with vdW-DF2, the bipyridine geometry is relaxed with PBE-D2, while upright amines (geometries **4**, **5**, and **6**) are constructed using the bond length and angle parameters of fully relaxed geometry **3**. All geometrical parameters as well as all atomic coordinates are summarized in Table S8 and section 12 in the Supporting Information.

After geometry optimization, the mean-field DFT eigenvalues and wavefunctions<sup>36</sup> are all computed using the PBE exchange-correlation functional with a 19-electron norm-conserving pseudopotential for Au. These eigenvalues and wave functions are used as the starting points for both the GW and DFT+ $\Sigma$  calculations.

**2.2. GW Calculations.** The many-electron self-energies for the quasiparticle eigenvalues are calculated within the GW approximation.<sup>9,35</sup> The GW approximation is based on perturbation theory, where a correction to the quasiparticle value is computed from a mean-field DFT starting point. The GW self-energy can be expressed as a sum of two terms, the screened exchange term and the Coulomb-hole term. Both of these terms can in turn be written as a function of the mean-field DFT eigenvalues and wave functions.<sup>36</sup>

In a typical one-shot GW calculation, the DFT wave functions and eigenvalues are used directly in the expressions for computing the GW self-energies. However, the DFT wave functions can be poor approximations to the quasiparticle wave functions for hybridized interfaces, and in principle, the self-energy matrix  $\Sigma(E)$  should be diagonalized to obtain a better approximation of the quasiparticle wave functions, which would

constitute a new starting point for perturbation theory (beyond one-shot GW calculations). The diagonalization of  $\Sigma(E)$  is a nontrivial task due to its energy dependence. Thus, there are few reports of GW calculations for hybridized molecule/metal interfaces. Here, instead of diagonalizing  $\Sigma(E)$ , we follow ref 37 and evaluate the self-energy in the basis of the molecular orbitals, as follows:

$$E_{\text{mol}}^{\text{QP}} = E_{\text{mol}}^{\text{GGA}} + \langle \varphi_{\text{mol}} | \Sigma(E) - V_{\text{xc}}^{\text{GGA}}(E) | \varphi_{\text{mol}} \rangle \quad (1)$$

We note that this is still a first-order perturbation theory approach. The motivation for our methodology is that the self-energy correction for metal states is negligible compared to that for molecular states, so that the self-energy operator  $\Sigma(E)$  is expected to be diagonal in the basis of molecular orbitals. (Here, we neglect the matrix elements in  $\Sigma(E)$  involving cross terms between the molecule and metal states, assuming these to also be small compared to the diagonal terms for the molecular orbitals.)

Within typical GW implementations, evaluating eq 1 requires the projection of the slab wave functions onto the molecular orbitals. Because we are investigating hybridized systems, where the molecular projected density of states (PDOS) plots show broadened molecular orbital peaks, the projection of slab wave functions onto the molecular orbitals is also helpful to define a single energy for the molecular orbital. Here, we define  $E_{\text{mol}}^{\text{GGA}}$  to be the energy level corresponding to the wave function with maximum projection on the MO. This method yields  $E_{\text{mol}}^{\text{GGA}}$  close to the peak maxima for the MOs in the PDOS plots, as shown in Figure S6.

We validate our procedures by (1) confirming that the self-energy operator is indeed approximately diagonal in the molecular basis (Tables S3–S5) and (2) showing that the GW self-energies match exactly those computed directly using GW, for states that are isolated completely within the molecular region.

GW self-energies involve long-range Coulomb interactions. Due to the 3D periodic boundary conditions used in the calculation, it is standard to use truncated Coulomb interactions in the evaluation of the self-energy for calculations with molecular or slab geometries.<sup>36</sup> The truncation of the Coulomb interactions affects only the self-energy evaluation and does not change the mean-field properties of the system, as evaluated within DFT. In this work, we use a “slab truncation” for the molecular layers, i.e., the Coulomb interaction is truncated in the direction normal to the slabs, so that the artificial presence of other slabs does not change the computed self-energies. To investigate the effect of intermolecular Coulomb interactions on the self-energy, we have also employed “box truncation”, where the Coulomb interaction is truncated in all three spatial directions. We note that this truncation does not affect the intermolecular Coulomb interactions in the DFT mean field calculations (including dipole–dipole interactions) or the vacuum potential; both are unchanged throughout the calculation.

**2.3. DFT+ $\Sigma$  Approach (Static Image Charge Screening).** The two-step DFT+ $\Sigma$  approach is introduced here to facilitate analysis of the self-energy effects. This approach adds a self-energy correction  $\Sigma$  to the DFT ELA for the molecule/metal system, evaluating  $\Sigma$  as the sum of two components: (1) the self-energy effects in the gas-phase isolated molecule and (2) the self-energy effects caused by the substrate, which is taken to be equal in magnitude to the substrate-induced image

charge energy when an electron is added to or removed from the molecule.<sup>7,8,30</sup> The DFT+ $\Sigma$  approach is based on GW calculations for the physisorbed system,<sup>13</sup> where it was proven numerically and shown analytically that, under certain assumptions, the substrate-induced change in self-energy for a single physisorbed molecule on a metal substrate is given by the image charge energy. Intuitively, one can understand this result as follows. The HOMO and LUMO levels of a molecule measure the amount of energy required to remove or add an electron to the molecule. In the presence of a metal substrate, the resulting hole/electron in the electron removal/addition process will be stabilized by screening from the metal substrate. In the physisorbed case, the screening effect from the substrate can be approximated with classical electrostatics as the image charge energy. This image charge energy makes it easier to remove and add electrons to the molecule, thus reducing the HOMO–LUMO gap. We note, however, that this simple picture ignores other substrate-induced exchange and correlation effects on the ELA.

The image plane position is taken to be 0.9 Å above the Au surface. Mulliken populations on each atom in the molecule are used for computing the image charge energy. The image charge energy thus computed is almost identical to that assuming a point charge in the middle of the molecule, except for geometry 11, where the sulfur atom (which contains 53% of the total charge) is located very close to the image plane (Table S10). Further details of methods are given in the Supporting Information.

### 3. RESULTS AND DISCUSSION

**3.1. GW Convergence of Absolute Energy Levels.** The accurate prediction of ELA in a hybrid system requires absolute (rather than relative) convergence of energy levels in the separate component systems; in particular, it is essential for GW to properly describe the Au(111) work function as well as the ionization potential (IP) and electron affinity (EA) of the molecules. While the DFT PBE Au(111) work function matches well with experimental results, achieving the same accuracy in GW is nontrivial.<sup>37</sup> However, for the parameters reported in this work (both slab truncation and box truncation), the work function for Au(111) obtained after GW self-energy corrections matches well with the PBE work functions (Figure S1). This is partly attributed to the very large 20 Ry cutoff energy for the dielectric matrix. Such a choice is also sufficient to converge the IP and EA for the gas-phase molecules (Table S2). In particular, we note that the benzene diamine (BDA) IP agrees well with experimental values and previous GW calculations.<sup>38</sup>

We note here that different approximations used to treat the  $\mathbf{q} \rightarrow 0$  limit in the GW self-energy calculations for metallic systems<sup>36</sup> result in different rigid shifts of all quasiparticle levels (Table S1). A careful calibration is therefore required for these ELA calculations. We note that the HOMO–LUMO gap (an easier quantity to converge) is computed to be the same in all these different approximations.

**3.2. ELA for Benzene Diamine (BDA) Molecular Layer on Au(111).** We begin our discussion with the ELA in BDA–Au(111) systems, where the HOMO alignment is known experimentally.<sup>39</sup> We consider different molecular orientations and coverage, as shown in Figure 1a. Geometries 1 and 2 are tilted structures with different coverage, while geometry 3, the face-on configuration, is constructed based on experimental information<sup>39</sup> and then fully relaxed using the vdW-DF2

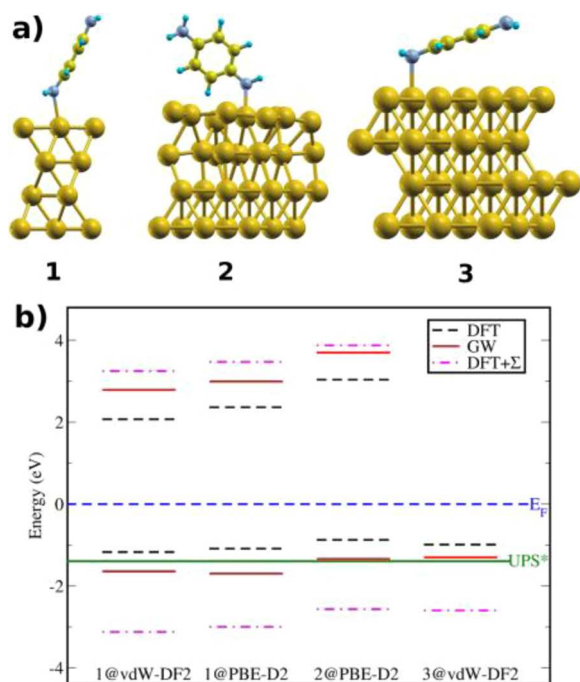


**Figure 1.** (a) Unit cell for BDA molecular layer on Au(111). Geometry 1:  $\sqrt{3} \times \sqrt{3}$  R30° Au cell. Geometries 2 and 3:  $3 \times 3$  cell. The gold, yellow, bright blue, and gray balls denote Au, C, H, and N atoms, respectively. (b) HOMO/LUMO ELA diagram obtained from GW, DFT, and DFT+ $\Sigma$ . The exchange-correlation functional used for geometry optimization is indicated. The experimental UPS HOMO position ( $-1.4 \pm 0.1$  eV) is from ref 39. Note that the LUMO level for geometry 3 is not spectroscopically defined (there is no clear peak when slab wave functions are projected onto the LUMO).

functional as implemented in VASP. In the relaxed geometry, the BDA molecule in geometry 3 is tilted 24° from the Au(111) surface, in excellent agreement with experimental near-edge X-ray absorption fine structure (NEXAFS) data.<sup>39</sup> Following prescriptions in the literature, the Coulomb interaction is truncated in the direction normal to the slabs during the evaluation of the GW self-energies (later referred to as “slab GW”).<sup>36,40</sup>

We focus first on the GW results, shown in red in Figure 1b. The GW HOMO alignment for geometry 3 is in good

agreement with the experimental ultraviolet photoelectron spectroscopy (UPS) value.<sup>39</sup> The HOMO alignments in geometries 1 and 2 are reasonably close to the UPS value as well, with very similar values for 1@vdW-DF2 and 1@PBE-D2. Moving to the DFT and DFT+ $\Sigma$  ELA (Figure 1b), we see that DFT (with PBE exchange-correlation functional) gives HOMO levels that are  $\sim 0.5$  eV too shallow compared to GW and UPS results, as expected from the underestimation of HOMO–LUMO gaps with DFT PBE. In contrast, the DFT+ $\Sigma$  HOMO levels are  $\sim 1.5$  eV deeper than the GW HOMO levels.

We note that our results appear to disagree with previous literature,<sup>39,41</sup> where the DFT+ $\Sigma$  ELA matched reasonably with the UPS result. There are several differences worth noting here. First, the atomic geometries used above are different from those in refs 39 and 41. The DFT ELA is very sensitive to the details of the atomic geometry, thus giving different DFT starting points for the calculation. Using the atomic geometries from the literature, we obtain the same DFT (PBE) HOMO alignment as in the references ( $-0.4$  eV for the BDA molecule, tilted 24° from the Au(111) surface, in a  $4 \times 4$  cell,<sup>39</sup> and  $-0.6$  eV for the linear chain motifs of BDA on Au(111)<sup>41</sup>). In comparison, our calculations show that geometry 3, which also has BDA tilted 24° from the Au(111) surface, but in a  $3 \times 3$  cell, has a DFT HOMO level of  $-1.0$  eV. The deeper DFT HOMO level for higher coverage is consistent with a net larger electrostatic potential shift for denser coverage due to a higher density of Au–N bond dipoles (upward with N losing charge to Au).<sup>25</sup> The sensitivity of the DFT HOMO alignment to atomic geometries leads to the question of whether the GW HOMO alignments are equally sensitive and whether or not the atomic geometries used in this work indeed correspond to the experimental geometry. Our calculations suggest that the GW ELA is fairly robust across geometries 1, 2, and 3, while ref 37 also gives a similar GW ELA for a BDA molecule physisorbed flat on Au(111), provided that the Fermi level is shifted to account for the error in the Au work function (there, the DFT PBE HOMO level was much shallower at  $-0.25$  eV). On the other hand, we have also performed a GW calculation on the linear chain motif geometry<sup>41</sup> and found a GW HOMO level of  $-0.75$  eV, which is much closer to  $E_F$  than the UPS value. Regarding the choice of geometries, we note that the linear chain motif geometry is stabilized by hydrogen bonds at 5 K<sup>42</sup> and is thus not likely to be the geometry in the room-

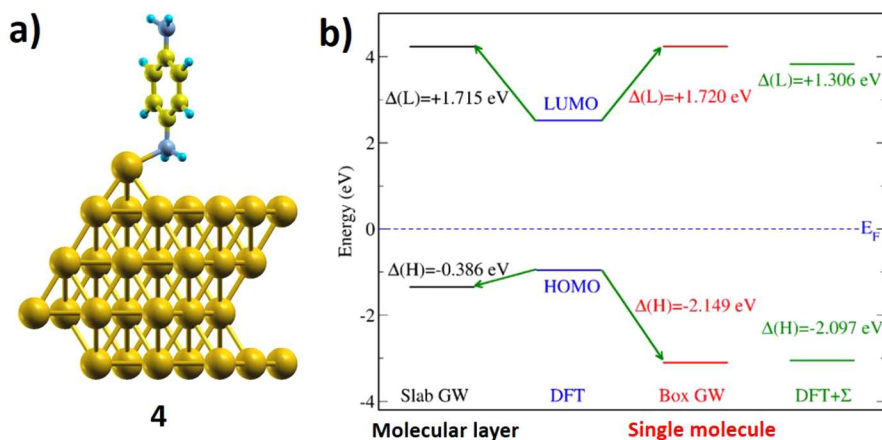


**Figure 2.** (a) Geometry 4: BDA oriented upright, bonded to a Au adatom in a  $3 \times 3$  Au(111) cell. (b) HOMO/LUMO ELA diagram obtained from GW, DFT, and DFT+ $\Sigma$ . Slab GW applies for the molecular layer, while box GW models the single-molecule limit.

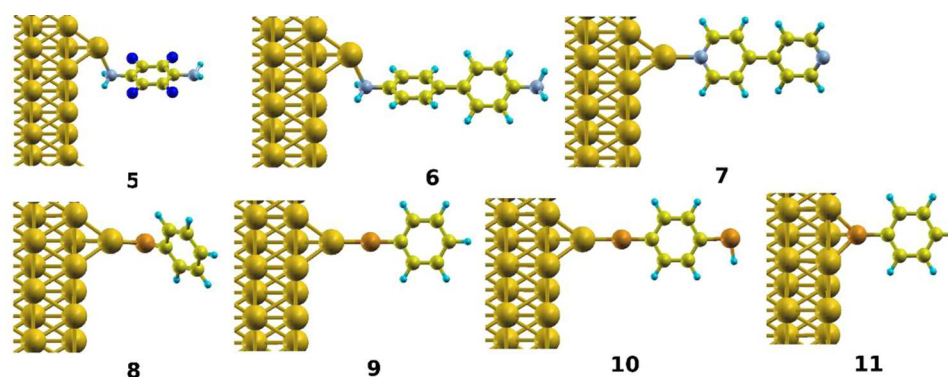


**Figure 3.** Geometries 5–11. Different molecules in a  $3 \times 3$  Au(111) cell. 5, fluorinated BDA (FBDA); 6, biphenyldiamine (BPDA); 7, 4,4'-bipyridine (BP); 8, 9, and 11: benzene thiol (BT); 10, benzene dithiol (BDT). In 5–10, the molecules are anchored on Au adatoms. In geometry 11, BT is anchored on face-centered cubic (fcc) hollow site of Au(111). Dark blue balls denote F, and orange balls denote S.

temperature UPS experiment.<sup>39</sup> Relaxing the BDA molecule in a  $4 \times 4$  cell results in a tilt angle of  $18^\circ$  (Figure S3) instead of  $24^\circ$  (the experimentally determined tilt angle), suggesting that the  $3 \times 3$  cell may be more appropriate. (See section 8 of the Supporting Information for more details.)

Another important difference is that here the image plane position is taken to be  $0.9 \text{ \AA}$  above the Au(111) surface, following a recent report that takes into account quantum mechanical exchange and correlation effects in the determination of the image plane position.<sup>43</sup> In contrast, the previous works used a classical image plane position of  $1.47 \text{ \AA}$  above the Au(111) surface,<sup>39,41</sup> thus giving much larger image charge corrections. In ref 27, we found that the quantum mechanical definition of the image plane is required to obtain ELA in good agreement with experimental scanning tunneling spectroscopy data for PTCDA on Au(111).

A comment about surface Au adatoms is in order here. We have also checked tilted and face-on configurations of BDA molecules anchored on Au adatoms on Au(111) and found scattered GW HOMO positions not matching the UPS value, indicating that the BDA molecules are not adsorbed on Au adatoms in the UPS experiment, consistent with the experimental report.<sup>39</sup>

**3.3. Molecular Layer versus Single Molecules.** Because DFT+ $\Sigma$  ELA was able to give a reasonable conductance for single-molecule BDA-Au junctions, we study a BDA-Au interface that is more representative of the single-molecule junctions, by anchoring BDA on Au adatoms (geometry 4; Figure 2a).<sup>44</sup> The GW HOMO level is still  $1.7 \text{ eV}$  closer to  $E_F$  than the DFT+ $\Sigma$  HOMO level. This result is in stark contrast to the excellent performance of DFT+ $\Sigma$  in predicting the conductance values of single-molecule BDA-Au junctions,<sup>7,8</sup> which in turn strongly suggests that DFT+ $\Sigma$  gives a reasonable ELA there (the conductance being extremely sensitive to the level alignment of frontier molecular orbitals relative to  $E_F$ ). Because our GW calculations are performed on geometries at fairly high coverage, we consider what happens if the Coulomb interactions between molecules are truncated when evaluating the GW self-energy (using a Wigner–Seitz box truncation scheme<sup>36,40</sup>). In that case, we find that the predicted HOMO level deepens by  $1.8 \text{ eV}$  and is much closer to the DFT+ $\Sigma$  result (Figure 2b). We call this “box GW” and note that similar truncation schemes have previously been used to describe other extended systems.<sup>45,46</sup> Due to the relevance of these results to single-molecule junctions, we also refer to these calculations as modeling a single molecule. However, we note that our model

does not strictly represent a single molecule on the Au surface, because intermolecular effects are already included at the DFT level.

Using box GW for geometry 2 with no Au adatom, we also find that the box GW and DFT+ $\Sigma$  HOMO levels match reasonably well (Table S11), thus indicating that the agreement between box GW and DFT+ $\Sigma$  does not depend on the presence of the Au adatom.

To assess the generality of our results and the dependence on the anchoring group, we consider other prototypical molecules, as shown in Figure 3. We focus on the MO levels relevant for transport in the corresponding single-molecule junctions (HOMO for amines and thiols, LUMO for pyridines). These anchoring groups have all been used extensively in single-molecule junctions, and thiols are also the anchoring group of choice in SAMs.<sup>47</sup> While the binding geometries for amines and pyridines are well-known, those for the more strongly interacting thiol-Au systems are surprisingly controversial.<sup>48,49</sup> Our choice of motifs for thiols on Au are far from exhaustive. The general consensus is that the S–H bond in the molecule cleaves upon adsorption on Au, forming a thiolate. This creates difficulties in our projection procedure; we find that using the radical orbitals as projectors leads to unphysical results, and we instead use the original thiol molecule for obtaining the MO projectors, which gives reasonable results (see Figure S6 for comparison of the projection method with the molecular PDOS). Bader charge analysis reveals a substantial intramolecular charge reorganization upon hydrogen cleaving and molecular adsorption, with the sulfur atom gaining an extra  $\sim 1.4e^-$  charge (Table S7). Despite the charge rearrangement, the HOMO levels of the thiolate molecules are not mixed with other MOs in the geometries considered here.

The level alignment results are shown in Table 1 and Figure 4. Remarkably, we find that, for all these systems, slab GW gives a level alignment that is significantly closer to  $E_F$  than DFT+ $\Sigma$ , indicating a large renormalization  $\Lambda$  coming from screening effects beyond simple image charge screening. In comparison with slab GW,  $\Lambda$  is very small in box GW, except for geometry 11 (benzenethiol anchored on the fcc hollow site) where  $\Lambda$  is  $1.5 \text{ eV}$ . The stark contrast between  $\Lambda$ 's computed for slab GW and box GW indicates that the additional screening effects in the molecular layer are related to intermolecular screening. Besides level alignment, we have also compared the molecular HOMO–LUMO gaps obtained with slab GW, box GW, and DFT+ $\Sigma$ . Except for geometry 11, the box GW and DFT+ $\Sigma$

Table 1. MO Levels, Referenced to  $E_F$ , for Geometries 5–11 (Units in eV)

	FBDA HOMO @geo.5	BPDA HOMO @geo.6	BP LUMO @geo.7	BT HOMO @geo.8	BT HOMO @geo.9	BDT HOMO @geo.10	BT HOMO @geo.11
DFT	-1.18	-0.76	+0.18	-0.27	-0.04	0.00	-1.26
DFT+ $\Sigma$	-3.33	-2.70	+1.51	-2.56	-2.41	-2.06	-2.07
box GW	-3.51	-2.94	+1.68	-2.22	-2.48	-2.55	-3.60
slab GW	-1.71	-1.17	+0.40	-0.72	-0.27	-0.34	-1.80

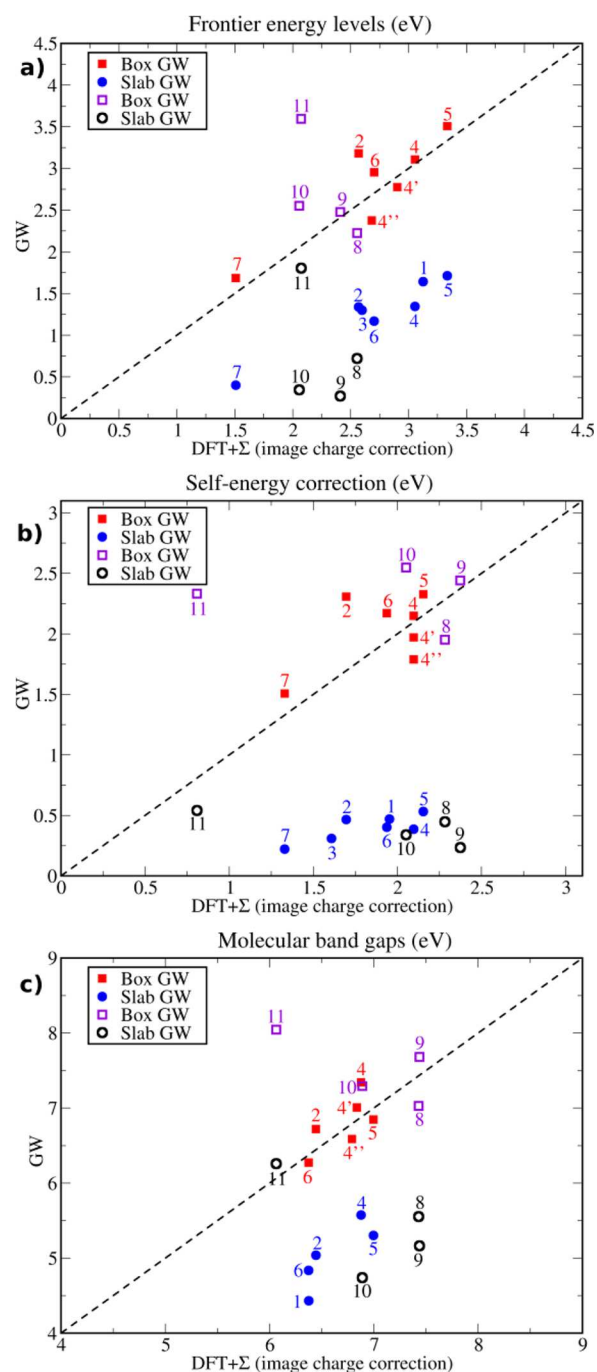


**Figure 4.** Scatter plots of (a) absolute frontier orbital energy levels relative to  $E_F$ , (b) magnitude of self-energy correction relative to DFT levels, (c) molecular HOMO–LUMO gaps: slab/box GW versus DFT + $\Sigma$ , indexed by geometry. The empty symbols in different colors denote thiolate/Au systems.

gaps agree reasonably well, while the slab GW gaps are  $\sim 1$  eV too small.

We also investigate two-sided metal/molecule/metal junction geometries for BDA with two different coverages, which are more representative of single-molecule junctions (Figure S4). For the  $\sqrt{3} \times \sqrt{3}$  R30° cell, we found a shallower slab GW HOMO level at  $-1.48$  eV, compared to a corresponding HOMO of  $-1.78$  eV for the one-sided interface. Both are much shallower than the DFT+ $\Sigma$  HOMOs of  $-2.95$  eV (two-sided) and  $-3.24$  eV (one-sided). The box GW and DFT+ $\Sigma$  HOMO

levels are also quite close in the  $3 \times 3$  cell junction ( $-2.15$  and  $-2.32$  eV, respectively).

Thus, for all geometries considered here, it is possible to draw two general conclusions. First, it is clear that there is a large additional energy renormalization for molecular orbital levels in chemisorbed molecular layers on Au(111), which goes beyond the picture of static image charge screening. Second, the box GW and DFT+ $\Sigma$  levels are in reasonable agreement, although with poorer agreement for the thiol in geometry 11. This suggests that static image charge screening can account for a large part of the substrate-induced electron self-energy effects in single-molecule junctions, explaining why DFT+ $\Sigma$  models could predict the electronic conductance in these systems.<sup>7,8,29–31</sup>

**3.4. Many-Electron Effects at Hybridized Molecule/Metal Interfaces.** **3.4.1. Single-Molecule Limit.** Given the above conclusions, a natural question to ask is why box GW and DFT+ $\Sigma$  levels agree reasonably well and whether or not this is a general result. To answer this question, it is instructive to revisit the following assumptions used in the analytical derivation of the DFT+ $\Sigma$  formalism for physisorbed single molecules on metal substrates:<sup>13</sup> (i) The molecular orbitals do not overlap with the metallic states; (ii) charge transfer between the molecules and the metal should be negligible; (iii) molecular polarizability is neglected; (iv) substrate-induced dynamical self-energy effects are neglected; and (v) the change in the screening potential upon molecular adsorption can be approximated by an image charge form. To what extent do the hybridized systems satisfy these assumptions?

We can show that assumption (i) may be relaxed to include hybridized molecule/metal systems in which the molecular orbitals (MOs) of interest do not mix with other MOs upon hybridization with the metallic states (slab wave functions with nonzero projections on the MO of interest should not have nonzero projections on other MOs). This is an important criterion and is found to be satisfied for all the MOs considered in Figure 4. The charge transfer between the molecule and the metal is negligible in our systems (Table S7). The effects of molecular polarizability are also small. The small molecular polarizability can be inferred from GW calculations for the molecular layer without the metal substrate, where the GW gap (8.0 eV) is very close to that of the single molecule (8.2 eV). We also note that, even when the intramolecular polarizability is large (such as for a PTCDA monolayer on Au(111)), the effect of molecular polarizability on the ELA is only a few tenths of eV.<sup>27</sup>

Assumptions (iv) and (v) are more difficult to verify without GW calculations on the full system. In particular, one should not expect DFT+ $\Sigma$  to give a high degree of quantitative accuracy in hybridized systems. However, it is clear from Figure 4b that a significant improvement over regular DFT calculations can be achieved, with self-energy corrections between 1.5 and 2.5 eV. Geometry 11 (thiol on hollow site) is an exception; we can trace the disagreement to an overly large image charge energy that results from the sulfur atom being very close to the Au(111) surface (charge rearrangements result in the sulfur atom carrying significant charge; Table S7). We have also performed additional box GW calculations for geometry 4, with another two layers of Au (4'), and also with a larger  $4 \times 4$  Au cell (4'') (slab GW calculations are too expensive for these geometries). The results are shown in Figure 4, with reasonable agreement between GW and DFT+ $\Sigma$ . Thus, static image charge effects can account for a large part of

the substrate-induced self-energy for many hybridized single-molecule/metal systems (Figure 4), providing a computationally efficient method (DFT+ $\Sigma$ ) to approximate the ELA in such systems.

**3.4.2. Substrate-Induced Intermolecular Self-Energy Effect.** What is the origin of the large additional level renormalization, beyond image charge screening, for molecular layers on Au(111)? Because this additional renormalization is absent in box GW calculations, we expect that intermolecular Coulomb interactions play a key role. We first ask if the intermolecular interactions could have resulted in additional band dispersion in GW. From Table S9, we can see that the HOMO energies at four high-symmetry k-points are essentially the same, suggesting that both DFT and GW HOMO levels are flat. Thus, the additional level renormalization affects the molecular orbital levels at all k-points equally and is likely to come from long-range intermolecular screening. On the other hand, the almost identical GW gaps for the isolated molecule and the molecular layer point to the importance of the metal substrate in mediating the additional screening.

To shed more light on the origin of this effect, we analyze the GW self-energies in terms of its two distinct components (screened exchange and Coulomb-hole terms)<sup>9,36</sup> (Table 2). The screened exchange term is the exchange interaction with the bare Coulomb interaction replaced by the screened Coulomb interaction, while the Coulomb-hole term is the interaction of the quasiparticle with the induced potential due

**Table 2. Components of the GW and Static COHSEX Self-Energy Corrections for Different Geometries, Together with the Bare Exchange Term (X)<sup>a</sup>**

	Method	X	SX	CH
HOMO for isolated BDA monolayer (no Au), with structure as in Geo. 4	Slab GW	-17.5	-10.2	-7.7
	Box GW	-17.6	-10.5	-7.1
BDA HOMO in Geo. 4	Slab GW	-15.9	-7.3	-8.0
	Slab static-COHSEX	-15.9	-7.2	-9.4
	Box GW	-17.5	-9.2	-7.9
	Box static-COHSEX	-17.5	-9.1	-9.7
BP LUMO in Geo. 7	Slab GW	-13.8	-5.4	-8.4
	Slab static-COHSEX	-13.8	-5.2	-9.5
	Box GW	-9.7	-4.0	-8.5
	Box static-COHSEX	-9.7	-4.2	-9.4
BT HOMO in Geo. 9	Slab GW	-13.6	-4.5	-8.5
	Slab static-COHSEX	-13.6	-4.1	-9.9
	Box GW	-15.4	-7.6	-7.6
	Box static-COHSEX	-15.4	-7.5	-9.3

<sup>a</sup>SX is screened exchange, and CH is the Coulomb-hole term. The GW self-energy is equal to the difference between (SX + CH) and the mean-field exchange-correlation term. The X term is given for comparison. Units are in eV, given to 1 d.p. for clarity (more data in Table S6).

to the rearrangement of electrons around the quasiparticle.<sup>9</sup> We also analyze the relative importance of static versus dynamical terms in the substrate-induced self-energy corrections by performing static COHSEX calculations<sup>36</sup> (which computes the screened exchange and Coulomb-hole self-energies in the static limits) and comparing those with the GW results.

*a. Hybridized Systems with Weak Chemisorption.* The data is qualitatively different for amines/pyridines compared to the more strongly bound thiols. Here, we associate the amines/pyridines with weak chemisorption, where no bonds are broken and the charge rearrangement upon adsorption is negligible. In contrast, the S–H bond in thiols is broken, leading to large intramolecular charge rearrangements—strong chemisorption. This distinction between weak and strong chemisorption scenarios has also been discussed in previous literature.<sup>46,50</sup>

We focus first on the former, where the Coulomb-hole term is essentially unchanged between the slab GW and box GW results (green; Table 2), so that the change in the GW self-energy, going from the single-molecule limit to the molecular layer, comes solely from the screened exchange term, which moves the frontier levels closer to  $E_F$  for the molecular layer (red versus blue; Table 2). In contrast, the screened exchange terms (and the Coulomb-hole terms) in the isolated BDA layer are similar for slab GW and box GW calculations (Table 2), further confirming that it is the presence of the Au substrate that renormalizes the intermolecular screening. We also see that most of the dynamical effects (differences between GW and COHSEX) come from the Coulomb-hole term, and that the screened exchange term is essentially the same in the GW and COHSEX calculations (red and blue; Table 2). Thus, the additional screening observed for weakly chemisorbed molecular layers is a static effect.

These observations allow us to propose a scheme (Figure 5a) to estimate the ELA in hybridized molecule/metal systems with weak chemisorption, such as when no bonds are broken, and no large charge rearrangements occur. An example would be chemisorption involving only donor–acceptor interactions (such as in amines/pyridines on Au). First, the ELA in the single-molecule limit (box GW) can be estimated using the DFT+ $\Sigma$  static image charge approach, as suggested by Figure 4. Next, one can account for the additional level renormalization for the molecular layer (slab GW versus box GW) by taking the difference between the static screened exchange terms computed using slab and box Coulomb truncation schemes (difference between red and blue in Table 2). While being just an estimate compared to the fully ab initio GW calculations, the proposed scheme is physically motivated by the data presented in this work and is computationally less expensive than GW, because the static screened exchange term involves only occupied states and is much easier to compute than the dynamical GW self-energy.<sup>51</sup> The results are shown in Figure 5b.

*b. Hybridized Systems with Strong Chemisorption.* For thiols, where the S–H bond in the molecule is broken upon adsorption on Au, the picture is more complex. The screened exchange term also moves the HOMO closer to  $E_F$  in slab GW compared to box GW; however, this is partially compensated by the Coulomb-hole term moving the HOMO in the opposite direction. This clearly shows that the self-energy effects for the more strongly bound thiolate/Au systems are qualitatively different from those of amines and pyridines on Au. Dynamical effects are also found to be significant.

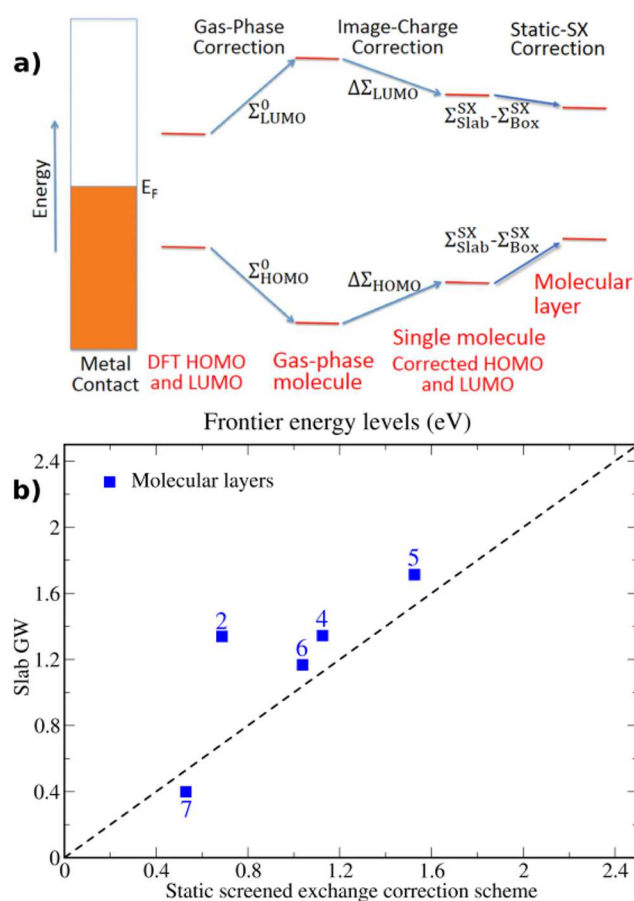


**Figure 5.** (a) Static screened exchange (SX) correction scheme upon the two step DFT+ $\Sigma$  method for molecular layer ELA on metal substrates. (b) Slab GW levels versus static SX corrected molecular layer energy levels. The screened exchange correction scheme only applies in the weak chemisorption case for amines and pyridine.

#### 4. CONCLUSIONS

Using state-of-the-art GW calculations with a projection approach, we have shown that the electron self-energy effects at hybridized molecule/metal interfaces are nontrivial. Our GW results on more than 10 geometries provide ab initio data to understand the physical origin of many-electron effects on the ELA at hybridized molecule/metal interfaces with weak and strong chemisorption. This physical understanding allows us to suggest computationally less expensive schemes to estimate the ELA for hybridized molecule/metal interfaces, except for the case of strongly chemisorbed molecular layers. Thus, despite an expected trade-off in quantitative accuracy, the proposed schemes can be used to obtain reasonable estimates for a large class of hybridized molecule/metal interfaces more efficiently, paving the way toward high-throughput analysis of structure–ELA relationships in such interfaces. The new insights into many-electron screening effects at hybridized molecule/metal interfaces also constitute an important step toward the understanding and manipulation of functional molecular/organic systems for both fundamental studies and applications.

We find that, when intermolecular Coulomb interactions are absent in the evaluation of the GW self-energy, the GW ELA agrees reasonably well with that predicted by the DFT+ $\Sigma$  image charge approach, for amines and pyridines on Au, and for some thiolate–Au geometries. This remarkable agreement explains the

excellent performance of the DFT+ $\Sigma$  approach in predicting the conductance of single-molecule junctions.<sup>7,8,29–31</sup> On the other hand, when intermolecular interactions are included, we uncover a huge (close to 1.5 eV) substrate-induced intermolecular screening effect that brings the frontier levels much closer to  $E_F$ . Good agreement is achieved with experimental UPS data for a BDA layer on Au(111). For weak chemisorption (amines and pyridines on Au), this substrate-induced intermolecular screening effect is a static effect manifesting itself in the screened exchange-interaction term. For strong chemisorption (thiolate/Au systems), substrate-induced dynamical self-energy effects and changes in the Coulomb-hole term are also important. As a final remark, we note that our results imply that if one were to compute the conductance of single-molecule junctions using GW, one has to be careful to truncate the Coulomb interactions between periodic copies of the molecules. In the literature,<sup>52–54</sup> the GW calculation is performed only for a finite region of the junction without including intermolecular screening effects. This also explains why the GW conductance was in reasonable agreement with experiment.

## ■ ASSOCIATED CONTENT

### ● Supporting Information

The Supporting Information is available free of charge on the ACS Publications website at DOI: 10.1021/acs.jpcc.7b00715.

Details of computation methods, GW projection, GW convergence of metal and molecule, GW self-energy off-diagonal elements, other geometries, decomposed GW versus static COHSEX, Bader charge analysis, binding energy, geometric parameters (including full atomic coordinates), DFT and GW bandstructure for isolated BDA layer, GW MO levels across the Brillouin zone, image charge correction amount, molecular PDOS, and table of all data (PDF)

## ■ AUTHOR INFORMATION

### Corresponding Author

\*phyqsy@nus.edu.sg.

### ORCID

Yifeng Chen: 0000-0003-4216-8242

### Notes

The authors declare no competing financial interest.

## ■ ACKNOWLEDGMENTS

S.Y.Q. and Y.C. acknowledge support from the Singapore National Research Foundation, Prime Minister's Office, under its medium-sized centre program and under Grant NRF-NRFF2013-07. I.T. acknowledges support from NSERC and SOSCIP. Computations were performed on the NUS Graphene Research Centre cluster. We thank Guo Li and Jeff Neaton for sharing the BDA linear chain model reported in the Supporting Information. We thank Keian Noori for discussions on related work.

## ■ REFERENCES

- (1) Heath, J. R. Molecular Electronics. In *Annual Review of Materials Research*; Annual Reviews: Palo Alto, CA, 2009; Vol. 39, pp 1–23.
- (2) Cuevas, J. C.; Scheer, E. *Molecular Electronics: An Introduction to Theory and Experiment*; World Scientific Publ. Co.: Singapore, 2010.

- (3) Galperin, M.; Nitzan, A. Molecular Optoelectronics: The Interaction of Molecular Conduction Junctions with Light. *Phys. Chem. Chem. Phys.* **2012**, *14*, 9421–9438.

- (4) Bergfield, J. P.; Ratner, M. A. Forty Years of Molecular Electronics: Non-Equilibrium Heat and Charge Transport at the Nanoscale. *Phys. Status Solidi B* **2013**, *250*, 2249–2266.

- (5) Ishii, H.; Sugiyama, K.; Ito, E.; Seki, K. Energy Level Alignment and Interfacial Electronic Structures at Organic Metal and Organic Organic Interfaces. *Adv. Mater.* **1999**, *11*, 605–625.

- (6) Braun, S.; Salaneck, W. R.; Fahlman, M. Energy-Level Alignment at Organic/Metal and Organic/Organic Interfaces. *Adv. Mater.* **2009**, *21*, 1450–1472.

- (7) Quek, S. Y.; Venkataraman, L.; Choi, H. J.; Louie, S. G.; Hybertsen, M. S.; Neaton, J. B. Amine-Gold Linked Single-Molecule Circuits: Experiment and Theory. *Nano Lett.* **2007**, *7*, 3477–3482.

- (8) Quek, S. Y.; Choi, H. J.; Louie, S. G.; Neaton, J. B. Length Dependence of Conductance in Aromatic Single-Molecule Junctions. *Nano Lett.* **2009**, *9*, 3949–3953.

- (9) Hybertsen, M. S.; Louie, S. G. Electron Correlation in Semiconductors and Insulators - Band-Gaps and Quasi-Particle Energies. *Phys. Rev. B: Condens. Matter Mater. Phys.* **1986**, *34*, 5390–5413.

- (10) Aryasetiawan, F.; Gunnarsson, O. The GW Method. *Rep. Prog. Phys.* **1998**, *61*, 237–312.

- (11) van Setten, M. J.; et al. Gw100: Benchmarking G(0)W(0) for Molecular Systems. *J. Chem. Theory Comput.* **2015**, *11*, S665–S687.

- (12) Jain, M.; Chelikowsky, J. R.; Louie, S. G. Reliability of Hybrid Functionals in Predicting Band Gaps. *Phys. Rev. Lett.* **2011**, *107*, 216806.

- (13) Neaton, J. B.; Hybertsen, M. S.; Louie, S. G. Renormalization of Molecular Electronic Levels at Metal-Molecule Interfaces. *Phys. Rev. Lett.* **2006**, *97*, 216405.

- (14) Garcia-Lastra, J. M.; Rostgaard, C.; Rubio, A.; Thygesen, K. S. Polarization-Induced Renormalization of Molecular Levels at Metallic and Semiconducting Surfaces. *Phys. Rev. B: Condens. Matter Mater. Phys.* **2009**, *80*, 245427.

- (15) Wold, D. J.; Haag, R.; Rampi, M. A.; Frisbie, C. D. Distance Dependence of Electron Tunneling through Self-Assembled Monolayers Measured by Conducting Probe Atomic Force Microscopy: Unsaturated Versus Saturated Molecular Junctions. *J. Phys. Chem. B* **2002**, *106*, 2813–2816.

- (16) Nijhuis, C. A.; Reus, W. F.; Barber, J. R.; Dickey, M. D.; Whitesides, G. M. Charge Transport and Rectification in Arrays of Sam-Based Tunneling Junctions. *Nano Lett.* **2010**, *10*, 3611–3619.

- (17) Xiao, X. Y.; Xu, B. Q.; Tao, N. J. Measurement of Single Molecule Conductance: Benzenedithiol and Benzenedimethanethiol. *Nano Lett.* **2004**, *4*, 267–271.

- (18) Quek, S. Y.; Kamenetska, M.; Steigerwald, M. L.; Choi, H. J.; Louie, S. G.; Hybertsen, M. S.; Neaton, J. B.; Venkataraman, L. Mechanically Controlled Binary Conductance Switching of a Single-Molecule Junction. *Nat. Nanotechnol.* **2009**, *4*, 230–234.

- (19) Kim, T.; Darancet, P.; Widawsky, J. R.; Kotiuga, M.; Quek, S. Y.; Neaton, J. B.; Venkataraman, L. Determination of Energy Level Alignment and Coupling Strength in 4,4'-Bipyridine Single-Molecule Junctions. *Nano Lett.* **2014**, *14*, 794–798.

- (20) Reed, M. A.; Zhou, C.; Muller, C. J.; Burgin, T. P.; Tour, J. M. Conductance of a Molecular Junction. *Science* **1997**, *278*, 252–254.

- (21) Heimel, G.; Romaner, L.; Bredas, J. L.; Zojer, E. Interface Energetics and Level Alignment at Covalent Metal-Molecule Junctions: Pi-Conjugated Thiols on Gold. *Phys. Rev. Lett.* **2006**, *96*, 196806.

- (22) Heimel, G.; Romaner, L.; Zojer, E.; Bredas, J. L. Toward Control of the Metal-Organic Interfacial Electronic Structure in Molecular Electronics: A First-Principles Study on Self-Assembled Monolayers of Pi-Conjugated Molecules on Noble Metals. *Nano Lett.* **2007**, *7*, 932–940.

- (23) Romaner, L.; Heimel, G.; Zojer, E. Electronic Structure of Thiol-Bonded Self-Assembled Monolayers: Impact of Coverage. *Phys. Rev. B: Condens. Matter Mater. Phys.* **2008**, *77*, 045113.

- (24) Verwuster, E.; Hofmann, O. T.; Egger, D. A.; Zojer, E. Electronic Properties of Biphenylthiolates on Au(111): The Impact of Coverage Revisited. *J. Phys. Chem. C* **2015**, *119*, 7817–7825.
- (25) Wang, J. G.; Prodan, E.; Car, R.; Selloni, A. Band Alignment in Molecular Devices: Influence of Anchoring Group and Metal Work Function. *Phys. Rev. B: Condens. Matter Mater. Phys.* **2008**, *77*, 245443.
- (26) Obersteiner, V.; Egger, D. A.; Zojer, E. Impact of Anchoring Groups on Ballistic Transport: Single Molecule Vs Monolayer Junctions. *J. Phys. Chem. C* **2015**, *119*, 21198–21208.
- (27) Zheng, Y. J.; et al. Heterointerface Screening Effects between Organic Monolayers and Monolayer Transition Metal Dichalcogenides. *ACS Nano* **2016**, *10*, 2476–2484.
- (28) Flores, F.; Ortega, J.; Vazquez, H. Modelling Energy Level Alignment at Organic Interfaces and Density Functional Theory. *Phys. Chem. Chem. Phys.* **2009**, *11*, 8658–8675.
- (29) Quek, S. Y.; Khoo, K. H. Predictive Dft-Based Approaches to Charge and Spin Transport in Single-Molecule Junctions and Two-Dimensional Materials: Successes and Challenges. *Acc. Chem. Res.* **2014**, *47*, 3250–3257.
- (30) Khoo, K. H.; Chen, Y. F.; Li, S. C.; Quek, S. Y. Length Dependence of Electron Transport through Molecular Wires - a First Principles Perspective. *Phys. Chem. Chem. Phys.* **2015**, *17*, 77–96.
- (31) Mowbray, D. J.; Jones, G.; Thygesen, K. S. Influence of Functional Groups on Charge Transport in Molecular Junctions. *J. Chem. Phys.* **2008**, *128*, 111103.
- (32) Grimme, S. Semiempirical Gga-Type Density Functional Constructed with a Long-Range Dispersion Correction. *J. Comput. Chem.* **2006**, *27*, 1787–1799.
- (33) Dion, M.; Rydberg, H.; Schroder, E.; Langreth, D. C.; Lundqvist, B. I. Van Der Waals Density Functional for General Geometries. *Phys. Rev. Lett.* **2004**, *92*, 246401.
- (34) Klimes, J.; Bowler, D. R.; Michaelides, A. Van Der Waals Density Functionals Applied to Solids. *Phys. Rev. B: Condens. Matter Mater. Phys.* **2011**, *83*, 195131.
- (35) Hedin, L. New Method for Calculating the One-Particle Green's Function with Application to the Electron-Gas Problem. *Phys. Rev.* **1965**, *139*, A796–A823.
- (36) Deslippe, J.; Samsonidze, G.; Strubbe, D. A.; Jain, M.; Cohen, M. L.; Louie, S. G. Berkeleygw: A Massively Parallel Computer Package for the Calculation of the Quasiparticle and Optical Properties of Materials and Nanostructures. *Comput. Phys. Commun.* **2012**, *183*, 1269–1289.
- (37) Tamblyn, I.; Darancet, P.; Quek, S. Y.; Bonev, S. A.; Neaton, J. B. Electronic Energy Level Alignment at Metal-Molecule Interfaces with a Gw Approach. *Phys. Rev. B: Condens. Matter Mater. Phys.* **2011**, *84*, 201402.
- (38) Sharifzadeh, S.; Tamblyn, I.; Doak, P.; Darancet, P. T.; Neaton, J. B. Quantitative Molecular Orbital Energies within a G(0)W(0) Approximation. *Eur. Phys. J. B* **2012**, *85*, 323.
- (39) Dell'Angela, M.; et al. Relating Energy Level Alignment and Amine-Linked Single Molecule Junction Conductance. *Nano Lett.* **2010**, *10*, 2470–2474.
- (40) Ismail-Beigi, S. Truncation of Periodic Image Interactions for Confined Systems. *Phys. Rev. B: Condens. Matter Mater. Phys.* **2006**, *73*, 233103.
- (41) Li, G.; Rangel, T.; Liu, Z.-F.; Cooper, V. R.; Neaton, J. B. Energy Level Alignment of Self-Assembled Linear Chains of Benzenediamine on Au(111) from First Principles. *Phys. Rev. B: Condens. Matter Mater. Phys.* **2016**, *93*, 125429.
- (42) Haxton, T. K.; Zhou, H.; Tamblyn, I.; Eom, D.; Hu, Z. H.; Neaton, J. B.; Heinz, T. F.; Whitlam, S. Competing Thermodynamic and Dynamic Factors Select Molecular Assemblies on a Gold Surface. *Phys. Rev. Lett.* **2013**, *111*, 265701.
- (43) Egger, D. A.; Liu, Z. F.; Neaton, J. B.; Kronik, L. Reliable Energy Level Alignment at Physisorbed Molecule-Metal Interfaces from Density Functional Theory. *Nano Lett.* **2015**, *15*, 2448–2455.
- (44) Venkataraman, L.; Klare, J. E.; Tam, I. W.; Nuckolls, C.; Hybertsen, M. S.; Steigerwald, M. L. Single-Molecule Circuits with Well-Defined Molecular Conductance. *Nano Lett.* **2006**, *6*, 458–462.
- (45) Spataru, C. D.; Ismail-Beigi, S.; Benedict, L. X.; Louie, S. G. Quasiparticle Energies, Excitonic Effects and Optical Absorption Spectra of Small-Diameter Single-Walled Carbon Nanotubes. *Appl. Phys. A: Mater. Sci. Process.* **2004**, *78*, 1129–1136.
- (46) Sau, J. D.; Neaton, J. B.; Choi, H. J.; Louie, S. G.; Cohen, M. L. Electronic Energy Levels of Weakly Coupled Nanostructures: C-60-Metal Interfaces. *Phys. Rev. Lett.* **2008**, *101*, 026804.
- (47) Vericat, C.; Vela, M. E.; Benitez, G.; Carro, P.; Salvarezza, R. C. Self-Assembled Monolayers of Thiols and Dithiols on Gold: New Challenges for a Well-Known System. *Chem. Soc. Rev.* **2010**, *39*, 1805–1834.
- (48) Pensa, E.; Cortes, E.; Corthey, G.; Carro, P.; Vericat, C.; Fonticelli, M. H.; Benitez, G.; Rubert, A. A.; Salvarezza, R. C. The Chemistry of the Sulfur-Gold Interface: In Search of a Unified Model. *Acc. Chem. Res.* **2012**, *45*, 1183–1192.
- (49) Hakkinen, H. The Gold-Sulfur Interface at the Nanoscale. *Nat. Chem.* **2012**, *4*, 443–455.
- (50) Thygesen, K. S.; Rubio, A. Renormalization of Molecular Quasiparticle Levels at Metal-Molecule Interfaces: Trends across Binding Regimes. *Phys. Rev. Lett.* **2009**, *102*, 046802.
- (51) Deslippe, J.; Samsonidze, G.; Jain, M.; Cohen, M. L.; Louie, S. G. Coulomb-Hole Summations and Energies for Gw Calculations with Limited Number of Empty Orbitals: A Modified Static Remainder Approach. *Phys. Rev. B: Condens. Matter Mater. Phys.* **2013**, *87*, 165124.
- (52) Jin, C. J.; Strange, M.; Markussen, T.; Solomon, G. C.; Thygesen, K. S. Energy Level Alignment and Quantum Conductance of Functionalized Metal-Molecule Junctions: Density Functional Theory Versus Gw Calculations. *J. Chem. Phys.* **2013**, *139*, 184307.
- (53) Strange, M.; Thygesen, K. S. Towards Quantitative Accuracy in First-Principles Transport Calculations: The Gw Method Applied to Alkane/Gold Junctions. *Beilstein J. Nanotechnol.* **2011**, *2*, 746–754.
- (54) Strange, M.; Rostgaard, C.; Hakkinen, H.; Thygesen, K. S. Self-Consistent Gw Calculations of Electronic Transport in Thiol- and Amine-Linked Molecular Junctions. *Phys. Rev. B: Condens. Matter Mater. Phys.* **2011**, *83*, 115108.